14:58:09 OCA PAD AMENDMENT - PROJECT HEADER INFORMATION 05/15/92

Active

Project #: E-18-655 Cost share #: Rev #: 6
Center # : R6561-0A0 Center shr #: OCA file #:
Work type : RES
Contract#: 0440670 Mod #: AMENDMENT 3 Document : CONT
Prime #: Contract entity: GTRC

Subprojects ? : N CFDA: N/A
Main project #: PE #: N/A

Project unit: MAT ENGR Unit code: 02.010.112
Project director(s):
SANDERS T H B JR MAT ENGR (404)894-5793

Sponsor/division names: PURDUE UNIVERSITY / WEST LAFAYETTE, IN
Sponsor/division codes: 400 / 087

Award period: 880401 to 910831 (performance) 910831 (reports)

Sponsor amount	New this change	Total to date
Contract value	2,300.00	70,687.00
Funded	2,300.00	70,687.00
Cost sharing amount		0.00

Does subcontracting plan apply ?: N

Title: INTEGRATING MATERIALS DESIGN INTO THE CAD/CAM ENVIRONMENT

PROJECT ADMINISTRATION DATA

OCA contact: Kathleen R. Ehlinger 894-4820

Sponsor technical contact

DR JAMES J SOLBERG
(317)494-7715

A A POTTER ENGINEERING CENT
PURDUE UNIVERSITY
WEST LAFAYETTE, IN 47907

Sponsor issuing office

MS ELIZABETH BOMBA
(317)494-1047

CONTRACT & GRANT BUSINESS A
PURDUE UNIVERSITY
WEST LAFAYETTE, IN 47907

Security class (U,C,S,TS) : U ONR resident rep. is ACO (Y/N): N
Defense priority rating : N/A N/A supplemental sheet
Equipment title vests with: Sponsor GIT X
NONE PROPOSED.
Administrative comments -
ISSUED TO ADD $2,300 AND EXTEND TERMINATION DATE TO 8/31/91.

GEORGIA INSTITUTE OF TECHNOLOGY
OFFICE OF CONTRACT ADMINISTRATION

NOTICE OF PROJECT CLOSEOUT

Closeout Notice Date 10/21/93

Project No. E-18-655_____ Center No. R6561-0A0_____

Project Director SANDERS T H B JR_____ School/Lab MSE_____

Sponsor PURDUE UNIVERSITY/WEST LAFAYETTE, IN_____

Contract/Grant No. 0440670_____ Contract Entity GTRC

Prime Contract No. _____

Title INTEGRATING MATERIALS DESIGN INTO THE CAD/CAM ENVIRONMENT_____

Effective Completion Date 910831 (Performance) 910831 (Reports)

Closeout Actions Required:	Y/N	Date Submitted
Final Invoice or Copy of Final Invoice	Y	920605
Final Report of Inventions and/or Subcontracts	Y	_____
Government Property Inventory & Related Certificate	N	_____
Classified Material Certificate	N	_____
Release and Assignment	N	_____
Other _____	N	_____

Comments_____
_____

Subproject Under Main Project No. _____

Continues Project No. _____

Distribution Required:

Project Director	Y
Administrative Network Representative	Y
GTRI Accounting/Grants and Contracts	Y
Procurement/Supply Services	Y
Research Property Managment	Y
Research Security Services	N
Reports Coordinator (OCA)	Y
GTRC	Y
Project File	Y
Other CARL BAXTER-FMD_____	Y
_____	N

NOTE: Final Patent Questionnaire sent to PDPI.

To be published in Diffusion Analysis and Applications
Editors: A.D. Romig, Jr. and M.A. Dayanada, TMS-AIME,
Warrendale, PA 15086, 1989.

Experimental Observations of and the Application of Growth Path Analysis to the Coarsening of δ' (Al_3Li) in Binary Aluminum-Lithium Alloys

T.H. Sanders, Jr.
and
A.M. Gokhale

School of Materials Engineering
Georgia Institute of Technology
Atlanta, Georgia 30332-0245

ABSTRACT

An overview of the experimental observations on the coarsening behavior of δ' precipitates in Al-Li alloys is presented. These observations demonstrate that the normalized particle size distributions reached a pseudo static form. Further, cube of the average particle size increases linearly with time, and the rate constant is sensitive to the volume fraction of the precipitates and the aging temperature. None of the coarsening theories explain all the quantitative and qualitative experimental observations in a self consistent manner. An alternate approach to the data analysis via growth path envelope technique shows that the local growth/shrinkage rate equation of LSW theory is not applicable to the coarsening behavior in these alloys. Further, the following equation for local growth/shrinkage rate of particles quantitatively describes the local kinetic behavior

$$\frac{dR}{dt} = \frac{K_o}{\lambda(t)} \left[\frac{1}{R^*} - \frac{1}{R} \right]$$

where, K_o is the kinetic constant, R^* is the critical particle size, and $\lambda(t)$ is a montonically increasing function of the process time.

Experimental Observations on δ' Coarsening

In the first of a series of publications by Gu et al. (1) the coarsening behavior of $\delta'(Al_3Li)$ in an Al-2.8Li-0.3Mn alloy (where the composition is given in approximate weight per cent) was discussed. The authors presented evidence that indicated that the growth of $\delta'(Al_3Li)$ obeyed Ostwald ripening kinetics. However, the interesting observations of that study showed that the shape of the experimental particle size distributions (PSDs) of the δ' phase was more symmetrical than the negatively skewed distribution predicted by many of the Ostwald ripening theories (2-5).

The Lifshitz-Slyozov-Wagner (LSW) theory (2,3), which predicts the coarsening kinetics and PSD of precipitates, is applicable only to dilute systems in which particle interactions are unimportant and furthermore the diffusion fields around individual particles do not overlap. There have been some modifications to the LSW theory that incorporate a volume fraction dependence of the coarsening rate and the shape of the PSDs (4-6). However, before a theoretical analysis can be tested, a comprehensive set of experimental PSDs is necessary so that comparisons of the various theories with experimental data can be made. In this regard the binary precipitation-hardening Al-Li system provides an ideal system (1). The δ' particles are coherent, have a small strain, are spherical, and can easily be imaged using centered dark field transmission electron microscopy (TEM) techniques. Furthermore, the large range of volume fractions which can be achieved in this system enables some of the important characteristics of the coarsening phenomenon to be followed as a function of composition.

To provide the necessary data to compare to the Ostwald ripening theories a series of binary Al-Li alloys were cast, fabricated, heat treated, and aged at a variety of aging temperatures and isothermal aging times. The results of these investigations are reported in detail elsewhere (7,8), but are summarized in this section.

Particle size distributions (PSDs) were determined for each alloy and aging condition using TEM. Increasing lithium content and temperature increases the rate of coarsening. The coefficient of variation (or the standard deviation of the normalized distribution) increases with increasing lithium content. The dilute alloys tended to have a negative coefficient of skewness ($CS<0$) whereas the higher content lithium alloys had $CS>0$. An alloy content of 2.8Li was close to a symmetrical distribution.

Another observation worth noting regarding the PSDs occurs when converting the frequency versus size histograms to a normalized histogram where the x-axis represents the parameter $D/\bar{D}$ where $\bar{D}$ is the average particle size for a given distribution. In Figures 1 and 2, comparisons of the longest and shortest PSDs for the two aging conditions are presented, and as illustrated in these figures the shape appears to be independent of aging time suggesting that the PSDs have achieved steady state.

To verify the steady-state nature of the PSDs the following scheme was adopted. The frequency of each normalized class interval was summed over the whole data set. For comparison with the individual normalized distributions, the composite histograms were normalized with respect to the maximum frequency. A comparison of the normalized composite histograms with the individual normalized histograms for the minimum and maximum aging times, for Al-2.4 Li and Al-4.5 Li are shown in Figures 3 and 4, respectively. There is good agreement between the form of the composite normalized distribution and the individual normalized distributions, suggesting that the distributions are steady state.

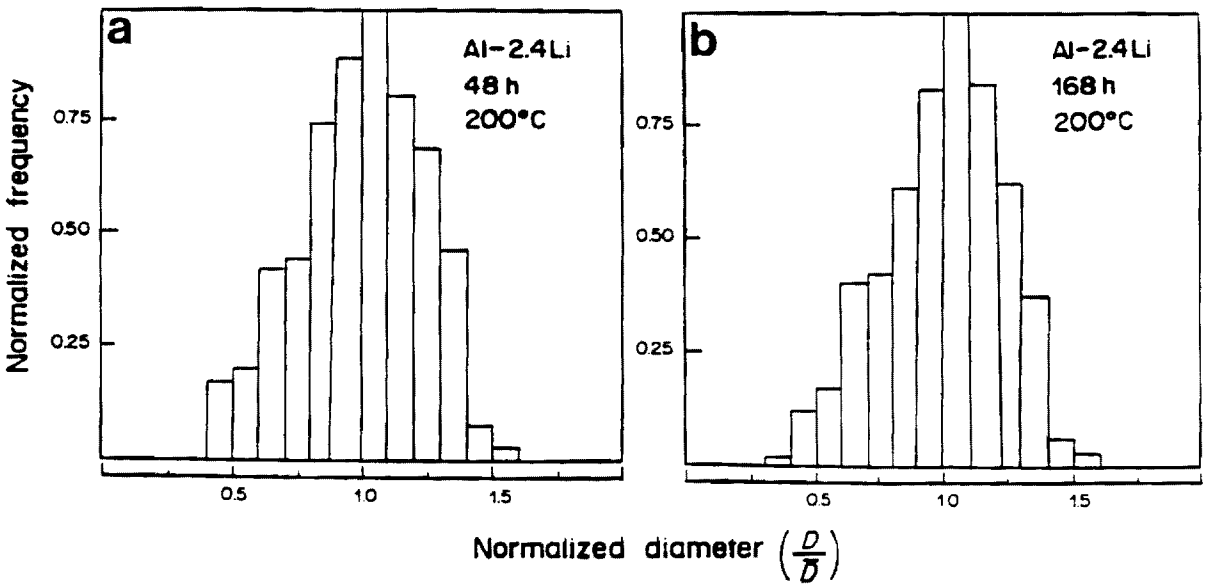

Figure 1. δ' PSD'S for Al-2.4 Li alloy showing a negatively skewed distribution (a) 200°C for 48 h and (b) 200°C for 168 h.

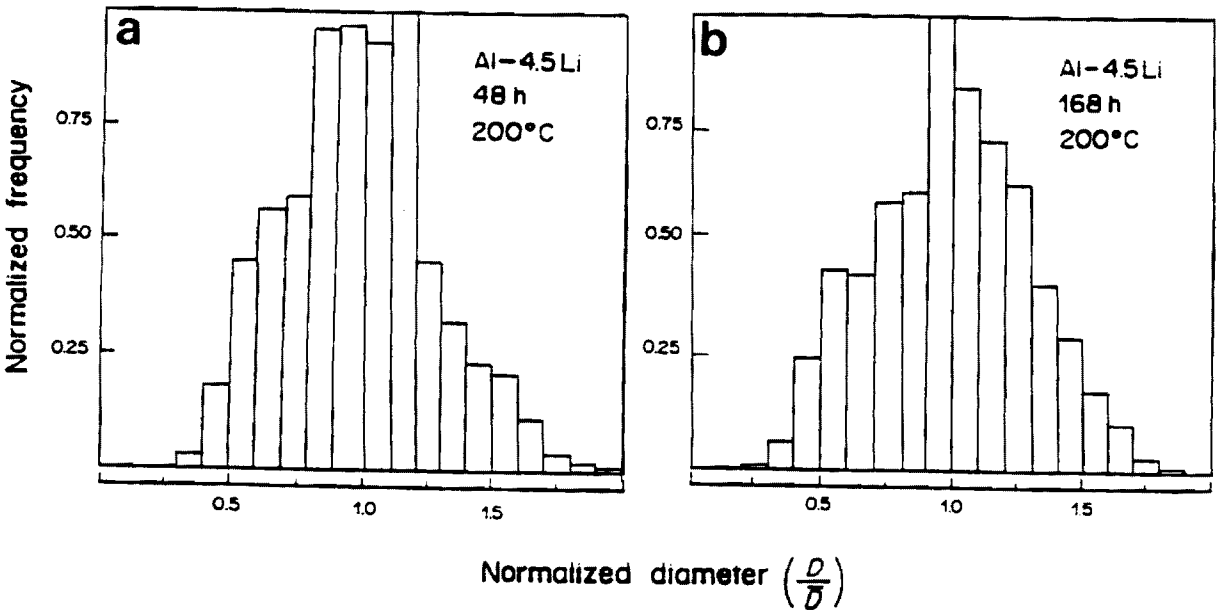

Figure 2. δ' PSD'S for Al-4.5 alloy showing a positively skewed distribution (a) Aged 200°C for 48 h, (b) aged 200°C for 168 h.

To compare the growth kinetics as a function of composition and aging temperature, the relationship between $\bar{R}^3$ and t for the different alloys and the two aging temperatures is shown in Figure 5. The growth rate constants for the analyses are plotted in Figure 6. The growth rate constants reported in (9,10) and constant calculated from the data of Williams (11) are also included in Figure 6. It was observed that the relationship between the growth rate constant and lithium content is approximately linear at 200°C and concave-up with increasing lithium content at 225°C.

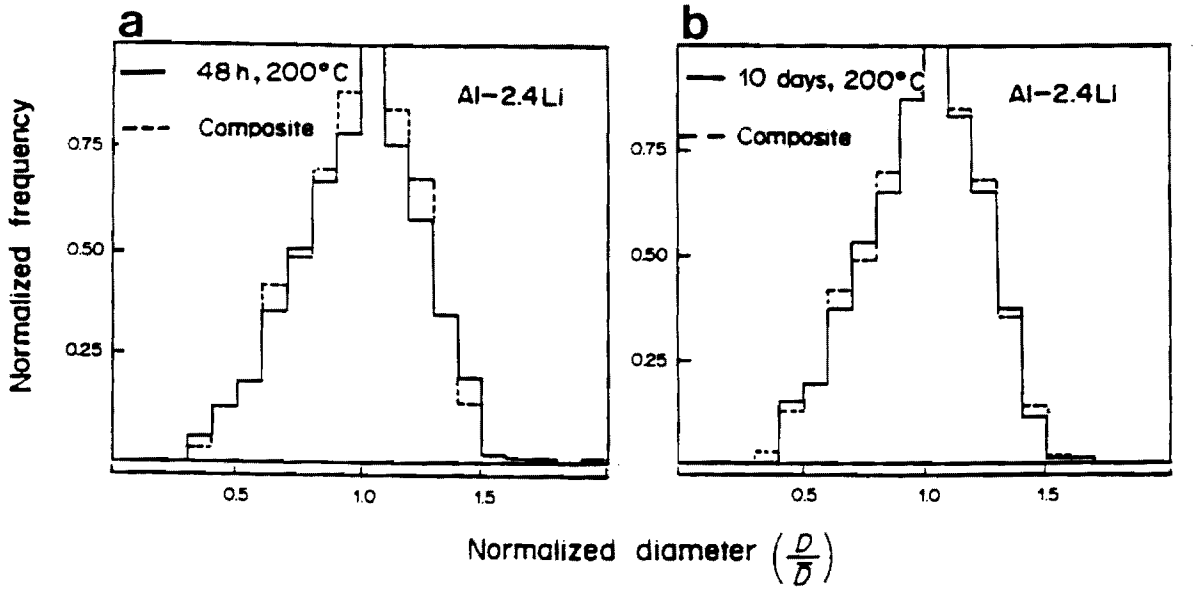

Figure 3. Comparison between the normalized composite histogram and the normalized histograms for Al-2.4 Li aged at 200° for (a) 48 h and (b) 10 days.

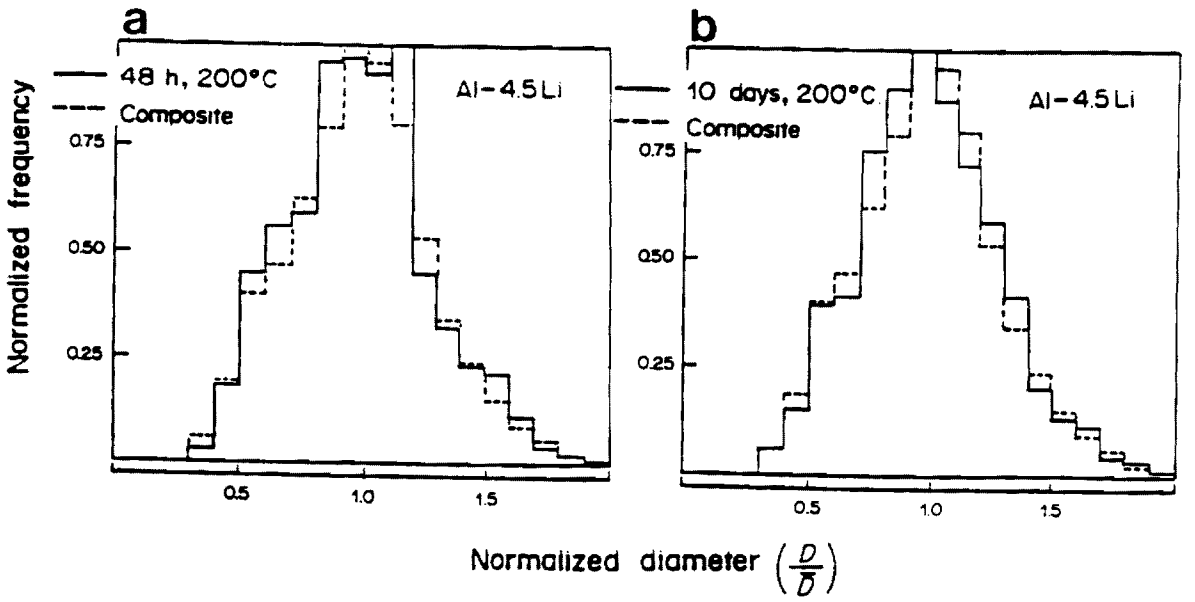

Figure 4.Comparison between the normalized composite histogram and the normalized histograms for Al-4.5 Li aged at 200°C for (a) 48 h and (b) 10 days.

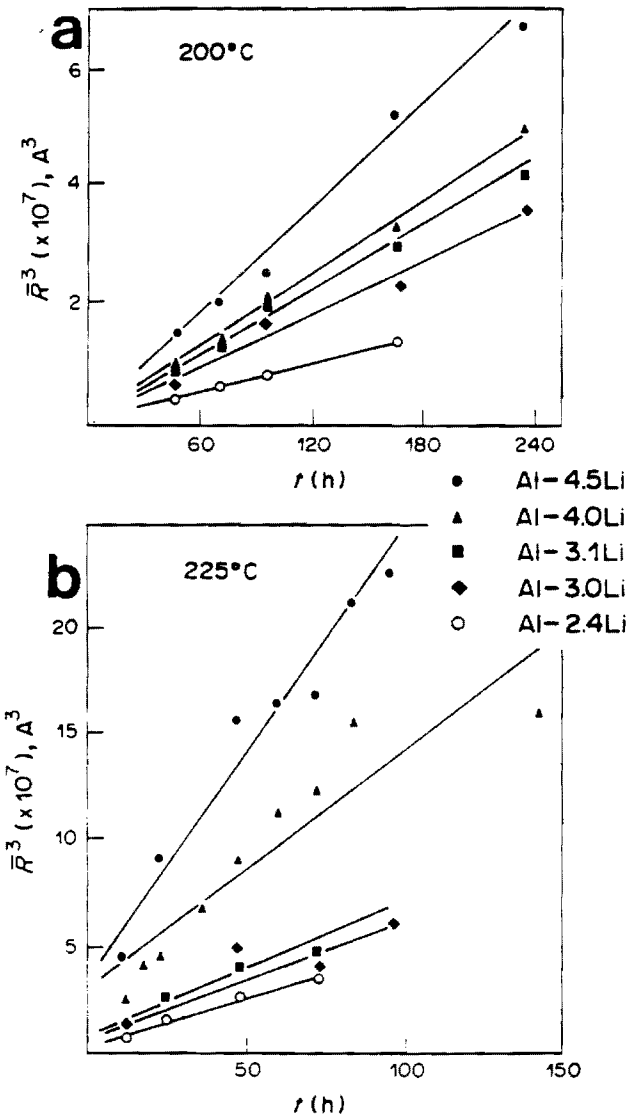

Figure 5. Plot showing the linear relationship between the cube of the average particle radius ($\bar{R}^3$) vs aging time (t) for different Al-Li alloys. (a) Aged at 200°C and (b) aged at 225°C.

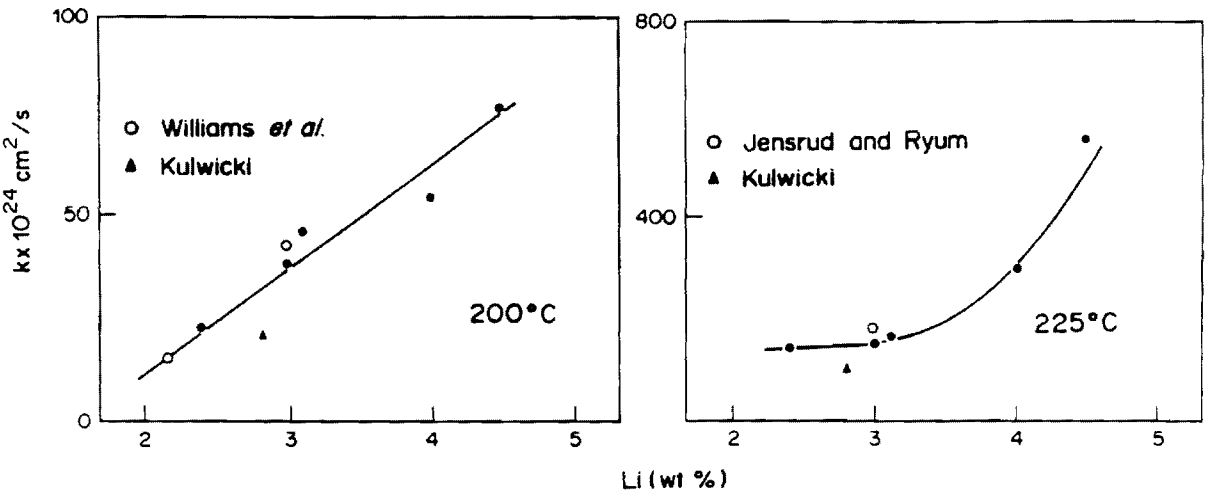

Figure 6. Plot of rate constant (k) vs Li content.

The combined effects of the Li content and aging temperature on the growth rate constant have been depicted in Figure 7 which shows a plot of the function ln kT vs 1/T. Data from other investigators has been included on that plot. A simple empirical expression relating lithium content, aging time and aging temperature was determined and has the form:

$$\ln kT = \frac{b}{T} + c. \qquad [1]$$

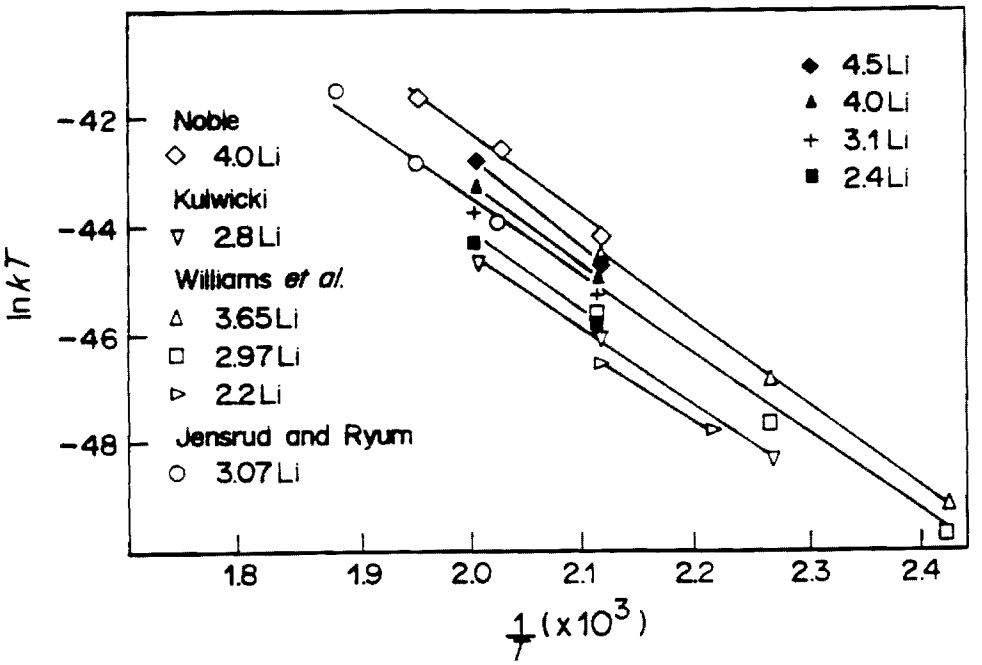

Figure 7.Plot of ln kT vs 1/T for various Al-Li alloys.

To determine whether a functional relationship exists between the average particle size $\bar{D}$ and the standard deviation, s, of the different distributions, these relationships were plotted for the different alloys. An example of such a plot for the Al-4.Li alloy is shown in Figure 8. Using linear regression analysis and a model of the form:

$$s = m\bar{D} + b \qquad [2]$$

where m and b are constants to be evaluated, the analytical expression for each alloy and aging temperature was determined. The value of b was approximately equal to zero. Figure 9 shows the linear regression lines without the data points. The linear relationships indicate that the width of PSD depends only on the extent of aging or the integrated effect of time and temperature. An interesting observation is that if the average value of CV for each alloy is plotted as a function of the volume fraction a linear plot is obtained and when extrapolated to zero volume fraction the coefficient of variation is that predicted by the LSW theory.

Since the form of the PSDs varied systematically with lithium content, the Weibull statistical distribution function was used to describe the δ' PSDs [7]. The Weibull distribution is widely used in the analysis of fatigue failure data and, recently, the Weibull distribution has been used to describe the steady state particle size distribution which develops during liquid phase sintering [12]. The power of this function lies in the fact that the shape of the distribution can be systematically varied using only two parameters when applying the analysis to a normalized size distribution.

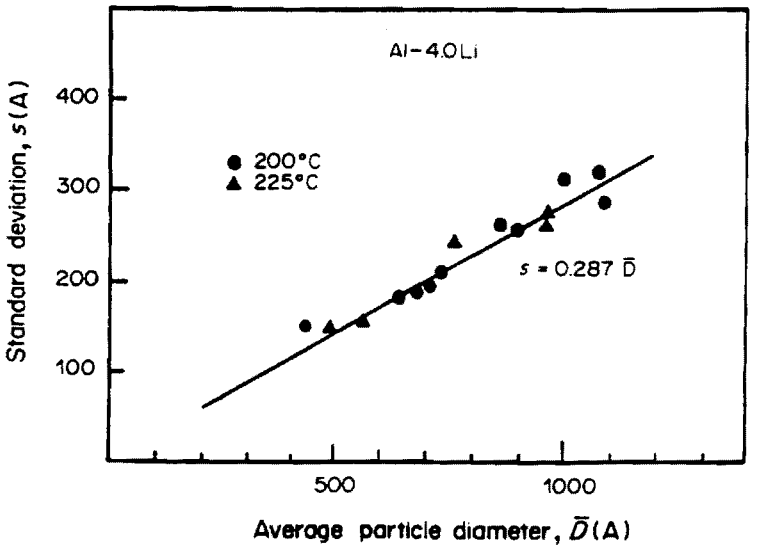

Figure 8. Standard deviation vs average particle diameter.

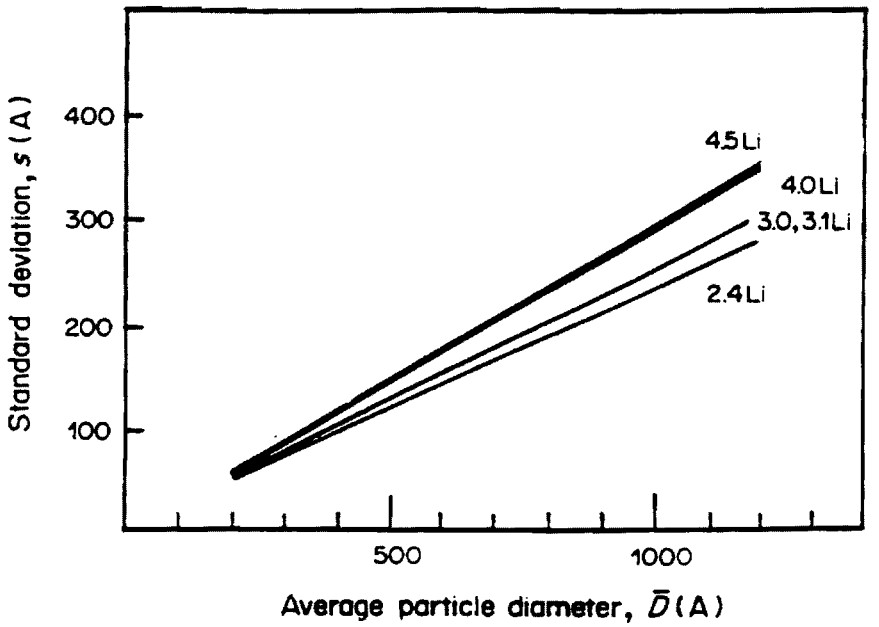

Figure 9.Plot showing the least-square lines for various Al-Li alloys.

A general form of the probability density of the Weibull distribution is given by

$$p(x) = \begin{cases} abx^{b-1} \exp(-ax^b) & \text{for } x>0,\ a>0,\ b>0 \\ 0 & \text{elsewhere} \end{cases} \quad [3]$$

and

$$\int_0^{+\infty} p(x)\, dx = 1 \quad [4]$$

The parameters a and b have been determined for each alloy and aging condition, and are plotted in terms of weight percent Li in Figures 10 and 11 [7]. A comparison of the experimentally determined PSDs and the calculated distribution are shown in Figure 12. A comparison of the Weibull fitted PSDs for various Al-Li alloys compared to the LSW distribution are shown in Figure 13.

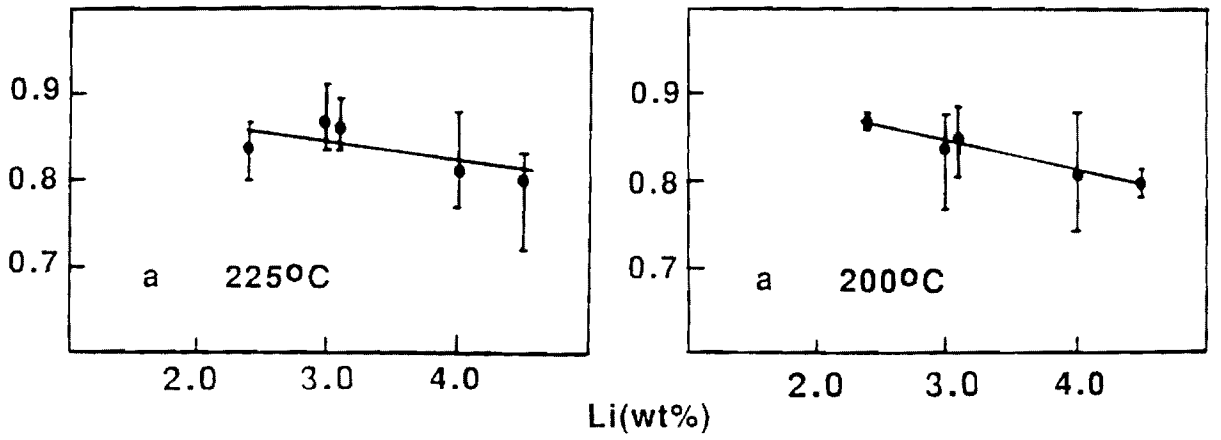

Figure 10. Relationship between the parameter a of the Weibull distribution and the lithium content for alloys aged at (a) 225°C and (b) 200°C.

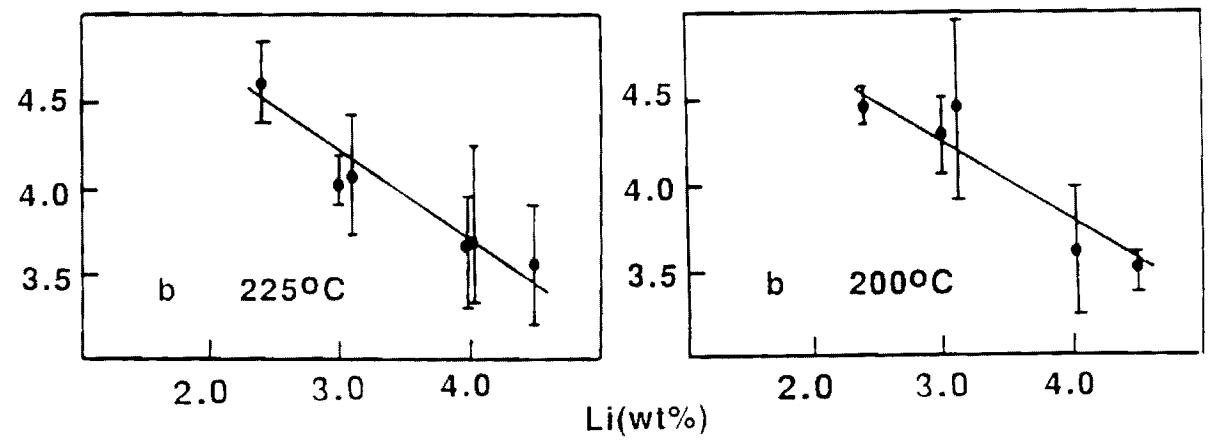

Figure 11. Relationship between the parameter b of the Weibull distribution and the lithium content for alloys aged at (a) 225°C and (b) 200°C.

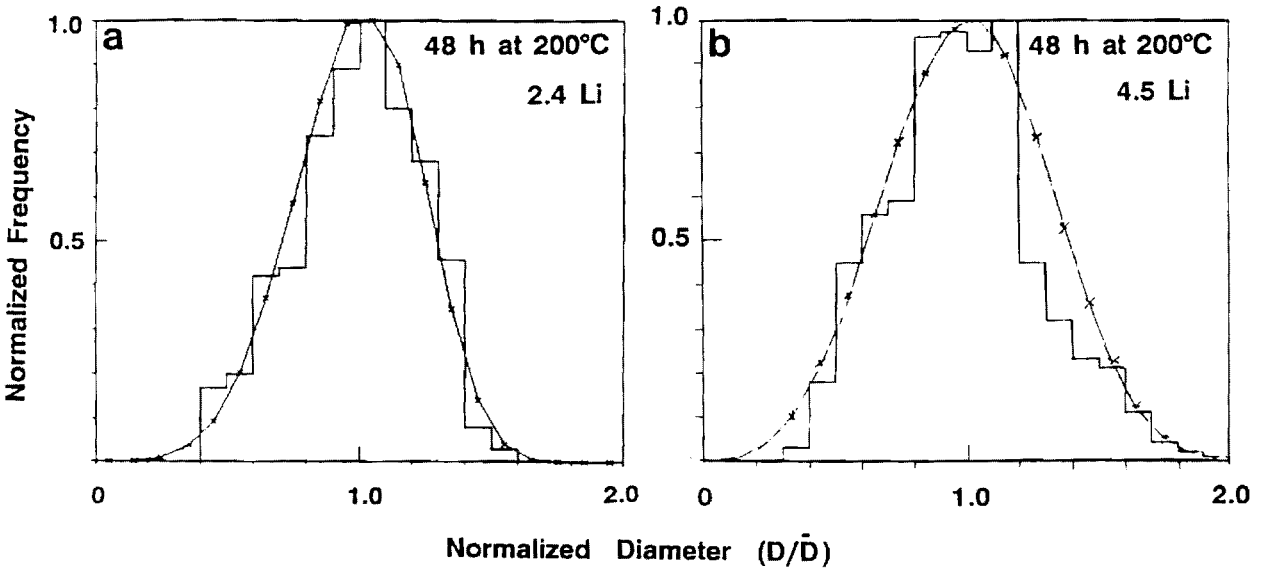

Figure 12. A comparison of the normalized histogram and generated Weibull distribution curve with calculated parameters a(= 0.868) and b(= 4.55) for Al-2.4Li alloy aged at 200°C for 48 h, and (b) for Al-4.5Li aged at 200°C for 48h where a = .805 and b = 3.46.

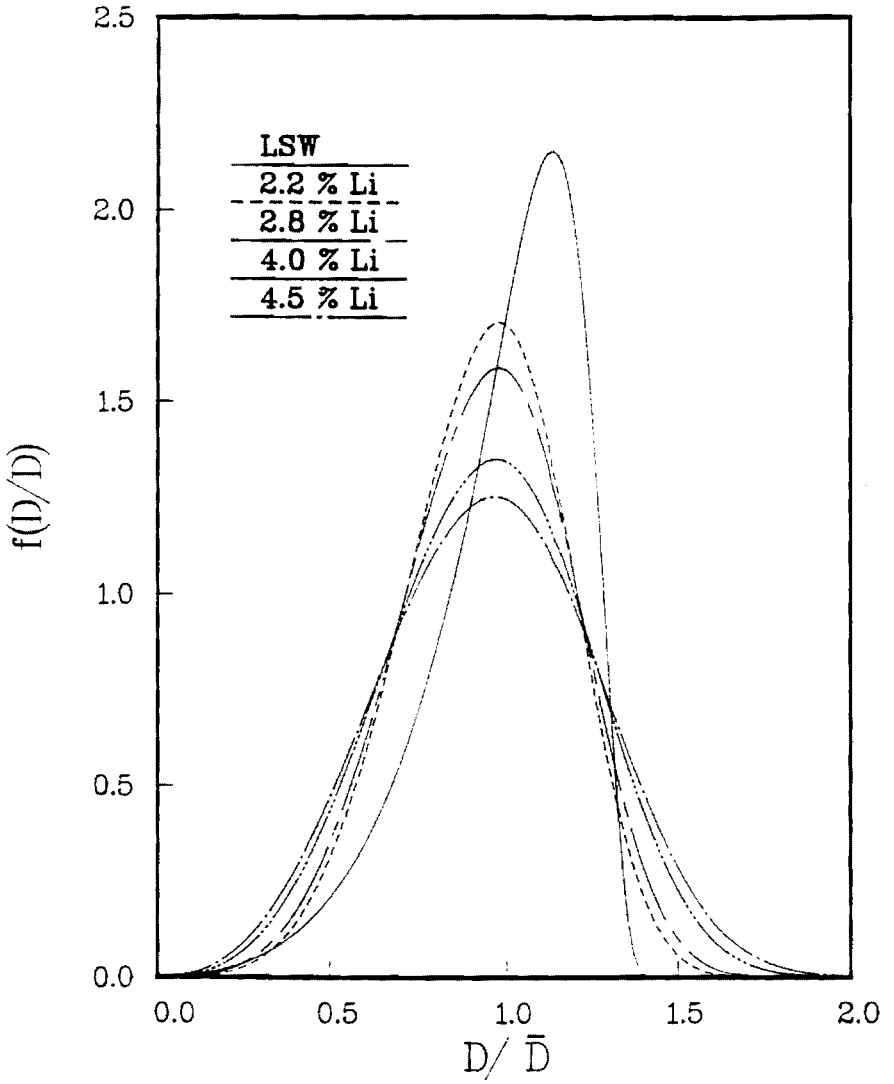

Figure 13 Comparison of Weibull generated normalized PSDS of a variety of Al-Li alloys with the LSW distribution.

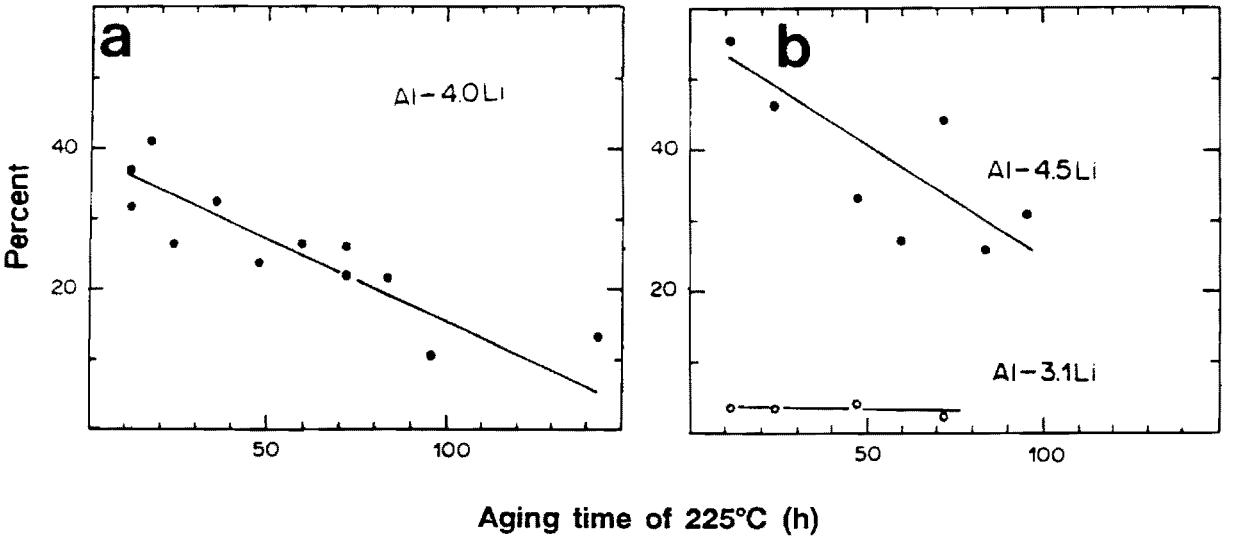

Figure 14. (a) The percent of particles with aspect ration ≤ 0.8 versus aging time for Al-4Li. (b) the percent of particles with aspect ratio ≤ 0.8 versus aging time for Al-4.5Li and Al-3Li.

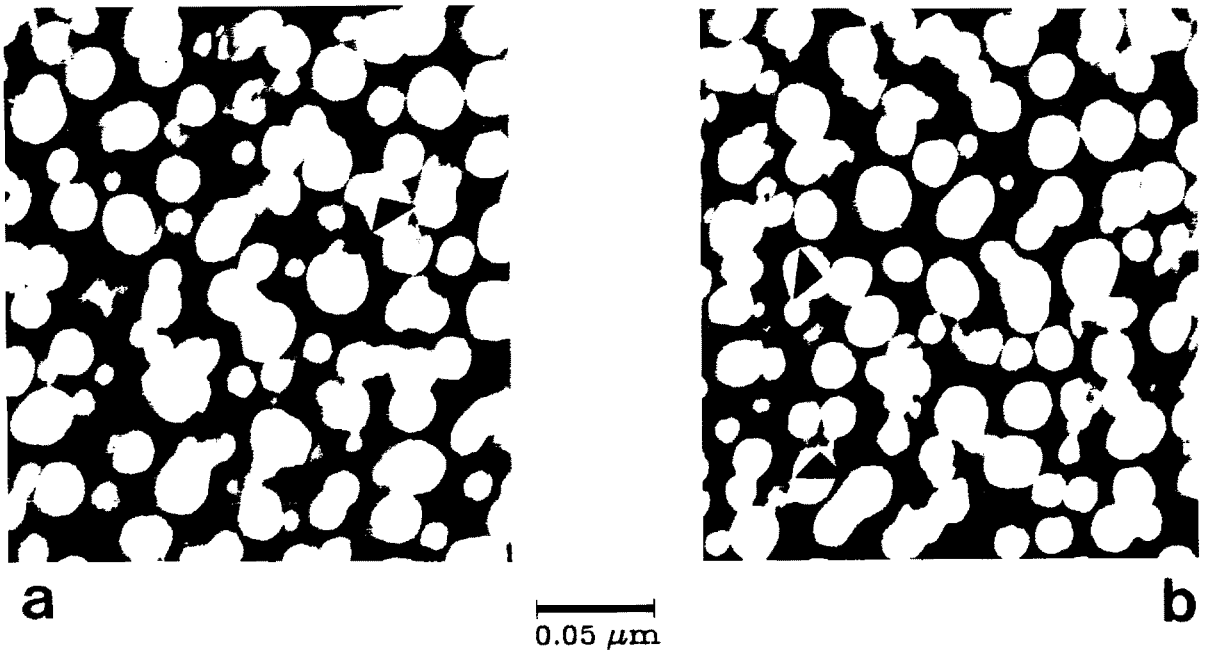

Fig. 15. TEM micrographs of Al-4.5Li alloy showing (a) coalesuence between a large and a small δ' particle. (b) Two δ' particles appearing to avoid one-another.

TEM investigations have shown that the morphology of δ' changes with compositions: increasing Li content results in particles that progressively lose their spherical morphology. To monitor the deviation from spherical morphology an aspect ratio of 0.8 was arbitrarily chosen as indicative of spherical morphology [8]. From a compilation of the number of particles with an aspect ratio of 0.8 for a given composition and aging condition a measure of the departure from spherical morphology can be estimated. This number was then followed as a function of aging time for a given aging temperature and composition. Figure 14a and b show the percent of particles whose aspects ratio is Figure 14b. It should be noted that regardless of the chosen aspect ratio the trend is the same; an increase in the aging time yields more particles which are spherical.

In more concentrated alloys, the non-spherical morphology of δ' particles seems to be brought about by encounters or coalesence among adjacent growing particles. Here the term ecnounters refers to the process by which the boundary of a particle expands outwards, approaching and eventually touching (encountering) another growing particle while maintaining a constant center-to-center distance. Figure 15a shows an apparent coalescence process between a large δ' particle and a smaller δ' particle. Particles which have obviously coalesced can be observed by the appearance of what is reminiscent of a sintering neck which occurs in hot pressed powders. However, examination of Figure 15b clearly shows that not all particles which are in close proximity to one another coalesce, and they may even tend to avoid one another. In more dilute alloys, the average interparticle-separation is large enough such that only a few particles can be encountered leading to the majority of δ' particles having spherical morphology.

Since the driving force for the coarsening process is the reduction of particle surface area per unit volume, two factors can work together to cause this reduction in particle surface area. The first factor is the growth of spherical particles with increasing aging time. A simple calculation shows that the reduction of surface area per unit volume is 16% with a 5 fold increase in aging time at 200°C. The second factor is associated with the transition of particle morphology from non-spherical to spherical with increasing aging time. A calculation for the Al-4Li alloy aged at 200°C shows that the reduction of surface area per unit volume is ~5% with a 5 fold increase of aging time. These calculations indicate that although the main factor for the reduction of particle surface area with increasing aging time is the coarsening of spherical particles, a small surface area reduction also occurs when the non-spherical particles become spherical.

In a recent publication of the coarsening in Al-Li alloys (8) comparisons between theory and experimental observations were made. In that paper, the LSW, the modified LSW, MLSW (proposed by Ardell(4), the so-called Lifshitz-Slyozov encounter modified (LSEM) model (6), Brailsford and Wynblatt model (5) and the Voorhees Glicksman model (13,4) were compared. Of the models surveyed the LSEM model was the only analysis which resulted in a good fit between the observed δ' PSDs and calculated PSDs. However, a cautionary remark should be made. When exmining Figures 2 and 4 we stressed the point that the PSDs for he 4.5Li alloy over the time interval investigated were steady state.

However, the shape of the δ' particles progressively became spherical with over aging. These two observations are contradictory. If the mechanism responsible for the shape of the PSD is controlled by a particular phenomemon the elimination of that process should result in change in the observed PSD.

The Al-Li system has given us the opportunity to follow the coarsening behavior of a second phase over a wide range of compositions and aging conditions. It has provided a set of consistent experimental observations on a system which is well behaved from the point of view of coarsening. The observations may be useful for theoreticians who are modeling the coarsening process since sufficient data over a wide range of compositions are available.

The important observations are summarized.

1. Increasing either lithium content or aging temperature increased the rate of coarsening.

2. Lithium content (volume fraction of second phase) determines the shape of the PSD. Increasing lithium content progressively changed the PSD from negatively skewed at low volume fractions to positively skewed at high volume fractions.

3. Over the experimental ranges investigated, the PSDs appear to be steady state distributions.

4. Increasing the volume fraction of δ' tends to make a significant number of particles nonspherical. The deviation from spherical morphology is attributed to particle encountering during the early stages of precipitation. However, increasing the aging time resulted in more spherical particles which is attributed to a reduction in the surface area as the particles became more spherical.

The above discussions demonstrate that none of the existing theories of diffusion controlled particle coarsening explain all the experimental observations pertaining to the coarsening of δ' precipitates in Al-Li alloys in a self consistent manner. The different theories of diffusion controlled particle coarsening basically differ in the boundary conditions utilized to solve the diffusion equation, and hence lead to different expression for local growth/shrinkage rate. With this input, the expressions for time dependence of average particle size and steady state size distributions are obtained by following exactly the same procedure. All the analytical models of particle coarsening involve an implicit assumption that the local growth/shrinkage rate of a particle is independent of its physical location in the sample. The computer simulation studies of Voorhees and Glicksman (14) demonstrate that the local growth/shrinkage rate of a particle indeed depends on its local surrounding, i.e., two particles of the same size and geometry at a given process time can have different values of local growth/shrinkage rate, depending on their location in the sample. Thus, the analytical models of particle coarsening can only represent the average kinetic behavior of a particle obtained by averaging the local particle growth rate of a particle of given size over all the possible locations in the matrix. Indeed, this description should be applicable to the

experimental data, because the manner in which the statistical sampling is carried out in the stereological measurements! The stereological measurements of particle size distributions (or any other geometrical properties) involve uniform (or random) sampling of the microstructure. The output data therefore represents the particle size distribution resulting from the averaging over all infinitesimal volume elements of the sample. Such an average particle size distribution can be thought of as the one evolved from the average local kinetic behavior quantified by an expression for average local growth/shrinkage rate. If this is accepted, then it is possible to extract the information concerning the average local growth/shrinkage rate from a set of experimentally measured particle size distributions by using the growth path analysis technique developed by DeHoff (15). Such an analysis can then lead to a self consistent expression for local growth/shrinkage rate which can explain all the experimental observations in a self consistent manner. The information can be also utilized to test different analytical models of particle coarsening at their roots. The growth path analysis involves the following basic steps.

(1) Measure the particle size distribution function $n_v(R,t)$ at different process times t.

(2) Recast the experimental data into an inverse cumulative distribution function $N_{v>}(R,t)$ as follows:

$$N_{v>}(R,t) = \int_{R}^{Rm} n_v(R,t)dR \qquad [5]$$

where, R_m is the size of the largest particle at time t. The quantity $N_{v>}(R,t)$ represents the number of particles of size larger than R at the process time t.

(3) Plot $N_{v>}(R,t)$ vs. R for different process times t.

(4) DeHoff (15) has shown that the pairs (R_i,t_i), which give the same value of $N_{v>}(R_i,t_i)$, essentially represent sizes R_i of the <u>same</u> particle in the evolving distribution at process times t_i. Thus, the cross cut (see Figure - 18) on $N_{v>}(R,t)$ vs. R plots at different t, taken at a constant value of $N_{v>}$, yields the size of the same particle at different process times, and hence it gives the growth path of that particle.

(5) Take the cross cuts on $N_{v>}(R,t)$ vs R plots at different t, for different constant values of the quantity $N_{v>}$, to generate the growth paths of different particles in the population.

The growth paths of different δ' precipitates in Al-4%Li alloy aged at 200°C were calculated in this manner. The set of growth paths contain complete information concerning the average local kinetic behavior of the δ' precipitates. The growth/shrinkage rate of each particle at a given time t can be calculated from the slopes of the corresponding growth paths. This yields the necessary input to study the average local kinetic behavior of the precipitates. Assume that the concept of critical particle size R* is applicable to the average local growth/shrinkage rate equation, where R* is determined by the particle size distribution.

Thus, at a given time, particles having size larger than R* grow, whereas the ones having size smaller than R* dissolve. Further, at a given time as R increases, dR/dt is expected to decrease (simply because a larger quantity of solute is required to increase the size of a larger particle by the same increment dR). The driving force for the coarsening process must montonically decrease with aging time. Thus, for a constant value of R, dR/dt must decrease as t increases or as R* increases. It may be said that dR/dt must be an odd function of the quantity (1/R* - 1/R) In the most simple case, dR/dt may be assumed to linearly depend on (1/R* - 1/R).

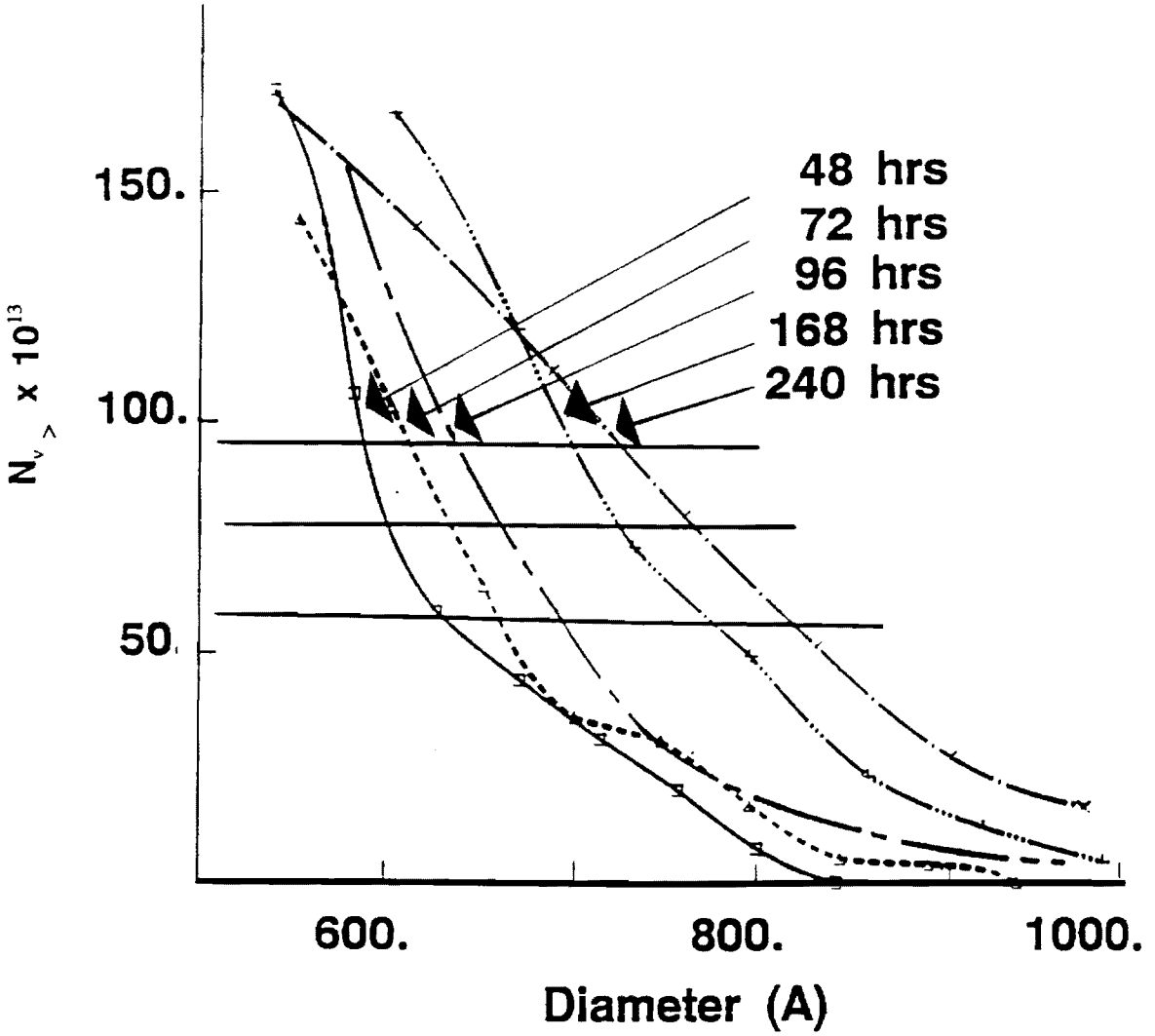

Figure 18. Application of growth path analysis.

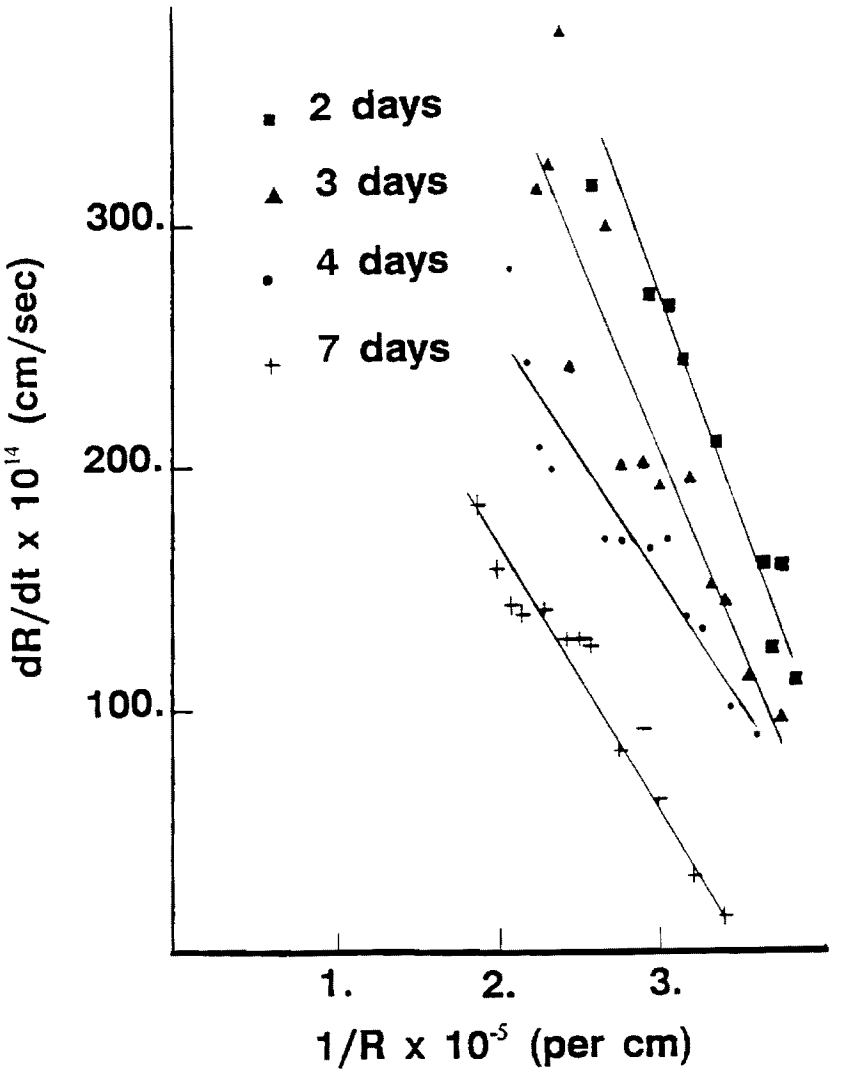

Figure 19. Plot of dR/dt vs 1/R during coarsening of δ' precipitates in Al-4%Li alloy at 200°C.

However, it may also further explicitly depend on R,R* and other geometric characteristics of the microstructure. The information concerning this functional dependence can be obtained by plotting dR/dt (i.e., local average growth/shrinkage rate obtained via growth path analysis) vs. 1/R at a fixed process time. Figure (19) depicts the corresponding behavior of the experimental data pertaining to Al-4%Li alloy aged at 200°C. Inspection of this figure leads to the following:

(1) Plot of dR/dt vs., 1/R is linear at the four process times studied

(2) The slope of the plot of dR/dt vs. 1/R decreases with time. Table-I, given the values of the slope at different values of t

(3) The x-axis intercept of the plot of dR/dt vs 1/R yields the critical size R* corresponding to that process time. Table-I reports these values of R*; the corresponding values of arithmetic average particle sizes are also reported.

Table - I
Values of the slope of $\frac{dR}{dt}$ vs $\frac{1}{R}$
and R* obtained from Figure 19

Aging time (days)	Slope cm^2/sec	R* (A°)	$\bar{R}$ (A°)
2	184×10^{-19}	225	216
3	164×10^{-19}	235	241
4	105×10^{-19}	223	275
7	109×10^{-19}	284	318

The above observations suggest the following functional form for the average local growth/shrinkage rate

$$\frac{dR}{dt} = \frac{K_o}{\lambda(t)} \left[\frac{1}{R^*} - \frac{1}{R} \right] \qquad [6]$$

where, K_o takes care of the parameters such as diffusion coefficient, surface energy etc. K_o is constant for an isothermal coarsening process. The parameter $(K_o/\lambda(t))$ is the slope of dR/dt vs. 1/R at given t. As this slope decreases with t, it follows that the quantity $\lambda(t)$ monotonically increases with t. It may be said that $\lambda(t)$ is proportional to the average distance through which the solute has to diffuse in the matrix for a particle to grow or shrink. It is experimentally observed that the cube of the average particle size varies linearly with t. In order for equation (6) to be compatible with this observation, $\lambda(t)$ must have dimensions of length. Note that, equation (6) obtained from the experimental growth paths has a functional form very different from the local growth/shrinkage rate equations of the analytical particle coarsening models in the literature. Diwan [16], and Gokhale, Iswaran and DeHoff [17] arrived at a similar functional form for local growth/shrinkage rate from the growth path analysis of the coarsening behavior in other alloy systems. Recently, DeHoff [18] has proposed a new theory of particle coarsening based on rigorous geometric considerations. It is interesting to note that the DeHoff's theory yields a local growth/shrinkage rate equation having a functional form identical to equation (6).

LSW theory of diffusion controlled particle coarsening gives the following equation for the local growth/shrinkage rate.

$$\frac{dR}{dt} = \frac{K_o}{R} \left[\frac{1}{R^*} - \frac{1}{R} \right] \qquad [7]$$

If this equation is applicable to the coarsening of δ' precipitates in Al-Li alloys, then a plot of (R. dR/dt) vs. 1/R should be linear at a given process time and such plots for different values of t should be parallel to one another. Figure (20) shows a plot of (R dR/dt) vs 1/R for the experimental data pertaining to the coarsening of δ precipitates in Al-4%Li alloy aged at 200°C. It is interesting to note that the plots of (R dR/dt) vs 1/R at different t are not parallel, and the slope of the least square lines decreases systematically with the process time. It follows that the basic local growth/shrinkage rate equation of LSW theory is not applicable to the coarsening behavior in this alloy.

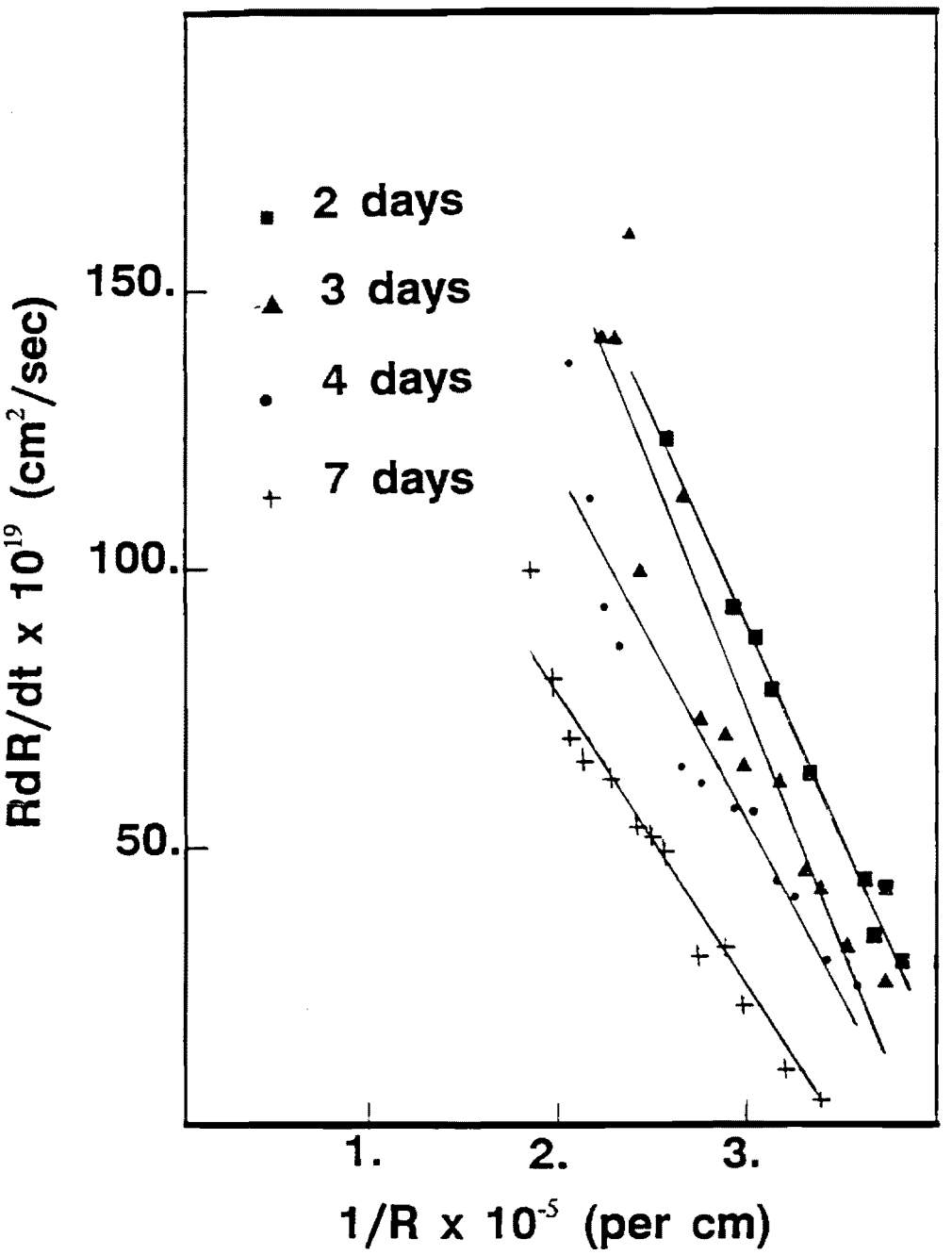

Figure 20. Plot of (R dR/dt) vs. 1/R during coarsening of δ precipitates in Al-4%Li alloy at 200°C.

References

1. B.P. Gu, J.H. Kulwicki, G.L. Liedl and T.H. Sanders, Jr., Mater. Sci. Eng., 70 (1985) 217.

2. I.M. Lifshitz and V.V. Slyozov, J. Phys. Chem. Solids, 19 (1961) 35.

3. C. Wagner, Z. Electrochem., 65 (1961) 581.

4. A.J. Ardell, Acta Metall., 20 (1972) 61.

5. A.D. Brailsford and P. Wynblatt, Acta Metall., 27 (1979) 489.

6. C.K.L. Davies, P. Nash and R.N. Stevens, Acta Metall., 28 (1980) 179.

7. B.P. Bu, G.L. Liedl, K. Mahalingam, and T.H. Sanders, Jr., Mater. Sci. Eng., 78 (1986) 71.

8. K. Mahalingam, B.P. Gu, G.L. Liedl, and T.H. Sanders, Jr., Acta Metall, 35 (1987) 483.

9. J.H. Kulwicki, M.S. Thesis, Purdue University (1983).

10. O. Jensrud and N. Ryum, Mater. Sci. Engng, 64 (1984) 229.

11. D.B. Williams and J.W. Edington, Metal Sci., 9 (1975) 529.

12. S. Takajo, W.A. Kaysser and G. Petzow, Acta Metall., 32 (1984) 107.

13. P.W. Voorhees and M.E. Glicksman, Acta Metall., 32 (1984) 2001.

14. P.W. Voorhees and M.E. Clicksman, Acta Metall. 32 (1984) 2013.

15. R.T. DeHoff: Metall. Trans, 1971, vol. 2, p.521.

16. R.M. Diwan: Ph.D. Dissertation, University of Florida, Gainesville, FL., 1974.

17. A.M. Gokhale, C.V. Iswaran, and R.T. DeHoff: Private Research, University of Florida, Gainesville, FL, 1979.

18. R.T. DeHoff: Private Communication.

Integration of Materials Design into the CAD/CAM Environment

Subtask: Microstructure Analysis

T.H. Sanders, Jr. and L. Collier

ABSTRACT

This subtask is a portion of an overall project directed at developing a CAD/CAM materials design model which utilizes material composition and processing parameters to predict microstructure and mechanical properties. The focus of this portion of the project is to model and quantify the microstructural features which control the specific engineering properties - strength, ductility, fracture toughness, fatigue crack growth resistance, and fatigue initiation resistance. An Al-2.6Li-.09Zr alloy has been chosen for this program and the microstructure is controlled by the extrusion process, post extrusion rolling, and solution heat treating and artificial aging. This alloy system is resistant to recrystallization, and exhibits extensive strain localization. The tendency to exhibits Planer deformation coupled with the unrecrystallized microstructure dramatically affect the properties of this alloy.

Integration of Materials Design into the CAD/CAM Environment

Subtask: Microstructure Development

T.H. Sanders, Jr. and L. Collier

ABSTRACT

This subtask is a portion of an overall project directed at developing a CAD/CAM materials design model which utilizes material composition and processing parameters to predict microstructure and mechanical properties. The focus of this portion of the project is to supply in-depth analysis of the microstructure components affecting properties.

The choice of the particular ternary Al-Li-Zr alloy that is the subject of this investigation was based upon four important considerations. First, the Al-Li systems represents an attractive alternative to conventional high strength alloys in that alloys contains lithium have lower density and higher elastic modului. Consequently, the aerospace community is very interested in this system. Second, the element responsible for both the reduction in density and the increase modulus is lithium, thus any viable alternative to an existing alloy must maximize the amount of lithium in the alloy. The presence of lithium has a dramatic effect on engineering properties such as toughness and fatigue crack growth in that it alters the deformation behavior by

promoting intense planar slip. This type of intense planar deformation does not occur to the same extend in other non-lithium containing aluminum alloys. Alloys with lithium contents in excess of 2 weight percent will show this type of deformation behavior. The presences of other alloying elements such as Cu and Mg (these elements along with Li are in 2090, 2091, 8090 and 8091) only modify the behavior, hence an alloy containing lithium as the primary solute would provide the understanding necessary to solve many of the problems unique to Al-Li without adding the complications of competing precipitation reactions. Third, the four commercial Al-Li alloys presently being marketed all contain zirconium as the recrystallization inhibiting dispersoid forming element. Fourth, quantitative data relating microstructure to composition, processing and properties existed prior to the initiation of this program on Al-Li, Al-Li-Mn, and Al-Li-Zr alloys, consequently to develop the methodology to predict properties from composition and processing, a well documented alloy system was considered necessary. Consequently, we have chosen an Al-2.8Li-.09Zr alloy for this investigation.

Research Objective

The objectives of this research are to isolate and identify specific microstructural features which are affected by processing and develop causal relationships between the microstructure and engineering properties.

Achievement

Several microstructural features have been identified as important to controlling the properties in this system, and they are summarized below.

1. Coarsening kinetics of the metastable, Al_3Li phase has been modeled and the results applied to strength.
2. The ordered nature of Al_3Li promotes planar deformation which leads to the development of intense planar deformation.
3. Impingement of the deformation bands at grain boundaries facilitates crack nucleation at boundaries.
4. The development of cracks at the boundaries coupled with the grain-boundary precipitate free zones leads to multiple cracks cracking and delamination toughening.
5. The recrystallizion to resistance of the alloy along with the shape change associated with the deformation process, leads to a highly elongated microstructure.
6. The strong crystallographic texture and the elongated grain structure combine to produce a microstructure with highly anisotropic properties.
7. The extensive planar deformation promotes stage I crack growth during constant amplitude cycling thus improving da/dn behavior at low an intermediate ΔK.
8. Crack bifurcation also improves crack growth resistance and fracture toughness when the loading direction is along the lamilar grain flow direction.

Integration of Materials Design into the CAD/CAM Environment

T. H. Sanders, Jr., B. M. Hillberry, A. F. Grandt, Jr., P. A. Blatt, J. M. Fragomeni, A. G. Gaitatzes, C. J. Hartshorn, J. A. Henkener, P. C. McKeighan, D. L. Ratzer, T. D. Scheumann, M. G. Valentine and G. J. Dail

Abstract

This research program is directed at developing an integrated computer model for designing materials. This model is based on an analytical prediction of the particle distribution of the microstructure as a function of the composition and the aging conditions. The additional processing variables, including extrusion ratio and extrusion temperature, are being incorporated into the model. From the microstructure, the critical resolved shear stress is being modeled and verified with experimental measurements of tensile strength. In addition, the fracture, fatigue and corrosion properties are being determined and incorporated into the model. The material being utilized for this study is a high-strength aluminum/lithium/zirconium alloy which has been provided by the Aluminum Company of America.

Research Objective

The objective of this research is to develop the methodology for integrating the design of materials into the CAD/CAM environment, whereby tensile, fatigue, fracture and corrosion properties can be predicted from the composition, heat treatment and processing variables.

Achievements

The microstructural model for predicting the particle size distribution of the δ' phase (Al_3Li) and the precipitation free zone in the Al-Li alloy system has been modified to include the extrusion processing variables, strain rate, extrusion temperature, heat generated during extrusion, reduction in area, die geometry and product geometry. The model predicts the δ' particle distribution used to directly predict the yield strength.

Development of the model for predicting the critical resolved shear strength from the microstructure has progressed. Microstructural mechanisms that contribute to the strengthening of precipitation hardened aluminum-lithium alloys containing type $L1_2$, ordered, coherent, spherical δ' (AL_3Li) precipitates have been examined. Optical along with transmission and scanning electron microscopy techniques were used to study the microstructure. The strengthening mechanisms considered were those which impede the conservative motion of dislocations. A number of existing models regarding particle shearing and looping mechanisms in precipitation hardened systems were evaluated. Order hardening was found to be the primary strengthening mechanism in the underaged, peak-aged, and overaged conditions and Orowan strengthening dominated the severly overaged condition. Using these strengthening mechanisms, the critical resolved shear strength and the yield strength have been predicted from the microstructure for the entire age hardening curve and compared to the experimental

measurements.

A computer program has been developed to link the microstructural and strength models. It is an interactive type program, user-friendly, executed on a SUN Workstation and mainly driven by a mouse input device. In order to plot the results from the Microstructure and Strength models as well as the Particle Distribution, the program employs the X11 window environment and a graphics package which has been developed at the Purdue Mechanical Engineering CADLAB. The SUN is also linked to an Apple Laser Writer enabling production of high quality output. The input to the program consists of the weight percent Li, the aging temperature and the peak aging time or any other time. The Microstructure model calculates the position of two hundred different size particles which are then displayed. It also calculates the precipitate free zone width which occurs in the overaged condition, the growth rate constant and the volume fraction of precipitate. The Particle Distribution subroutine takes the particles and calculates the coefficients of variance, skewness and kurtosis. The Strength Model calculates the plots the yield and ultimate tensile strengths.

The integration of a computer, software and a materials testing machine has assisted in the development of a tensile model by performing data acquisition and analysis of results from a standard tensile test. The Sun 3/180 Workstation has enabled the user to analyze and make accurate conclusions immediately following the actual test. Also, on-line recording documents all tensile tests performed and stores the test results in a flexible database. Presently, five processing variables have been examined in this data acquisition phase of the project. Tensile properties have been experimentally determined as a function of extrusion ratio, specimen orientation, aging temperature, extrusion geometry, and extrusion temperature. The extrusion geometry resulted in the most dramatic differences in tensile behavior. The round specimens had a significant higher yield strength when compared to the flat specimens with the same processing variables. The peak-age yield strength for the round extrusion was approximately 20 ksi higher than that of the flat material. However, the flat specimens exhibited greater elongations and less sensitivity to aging time past one hour aging. For either flat or round material, extrusion temperature did not significantly effect either the aging response or the magnitude of the tensile properties. Little noticeable difference is apparent in either ductility or yield strength. Tensile behavior was also unchanged by varying extrusion ratio.

To assist with the development of the fatigue model, a database of fatigue properties, including both crack initiation and crack propagation properties, is being compiled for the Al-2.6Li-0.09Zr alloy. Constant load amplitude fatigue crack growth tests at R=0.1 have been completed in both the L-T and T-L orientations for the Al-Li-Zr material using C(T) specimens and on reference alloys 7075-T651 and 2090-T8E41. In addition, crack growth rate data at different stress ratios have been obtained using the four-point bend specimen geometry in the L-T orientation. The fatigue crack profiles of the Al-Li-Zr specimens oriented in the T-L direction were characterized by extensive crack branching and deflections at approximately 45° to the direction of expected crack growth. Branching and deflection were observed to be less severe in the L-T specimens. The Al-Li-Zr alloy was determined to be more resistant to crack growth at low ΔK levels when compared with the 7075 and 2090 reference materials. Also, anisotropic fatigue crack growth behavior was observed in both aluminum-lithium alloys, with more resistance to crack growth in the T-L orientation than in the L-T orientation. A comparison of the data obtained from the Al-Li-Zr and 7075 bend specimens indicated that the Al-Li-Zr material is influenced more than the 7075 by increasing the stress ratio.

The fracture mechanism for this alloy is being examined experimentally. Fracture tests performed indicate that the alloy exhibits high energy, high toughness fracture behavior with tortuous, non-planar fracture surfaces. The thickness independent fracture behavior observed is very different from traditional alloys and indicates some important considerations with respect to fracture mode. The testing performed on the alloy has been directed at determining the fracture mode and the variables influencing it. Studies of the fracture surface and subsurface microstructure of fractured specimens indicate highly localized slip planes through the lamellar oriented grains with cracking along the columnar grain boundaries. Considerable secondary cracking has been observed. These observations provide insight into the fracture mechanism which will aid in the development of a fracture prediction model.

This project is divided into a series of subtasks, each being investigated by a Graduate Research Assistant. The following reports by the Graduate Research Assistants describe in detail the objectives and achievements for each of these subtasks.